


Hidden interplay of current-induced spin and orbital torques in bulk Fe₃GeTe₂Tom G. Saunderson ^{1,2,*} Dongwook Go ^{1,2} Stefan Blügel ² Mathias Kläui^{1,3} and Yuriy Mokrousov^{1,2}¹*Institute of Physics, Johannes Gutenberg University, 55099 Mainz, Germany*²*Peter Grünberg Institut and Institute for Advanced Simulation, Forschungszentrum Jülich and JARA, 52425 Jülich, Germany*³*Centre for Quantum Spintronics, Department of Physics, Norwegian University of Science and Technology, 7491 Trondheim, Norway*

(Received 19 May 2022; accepted 5 September 2022; published 7 November 2022)

Low crystal symmetry of magnetic van der Waals materials naturally promotes spin-orbital complexity unachievable in common magnetic materials used for spin-orbit torque switching. Here, using first-principles methods, we demonstrate that an interplay of spin and orbital degrees of freedom has a profound impact on spin-orbit torques in the prototypical van der Waals ferromagnet Fe₃GeTe₂. While we show that bulk Fe₃GeTe₂ hosts strong “hidden” current-induced torques harvested by each of its layers, we uncover that their origin alternates between the conventional spin flux torque and the so-called orbital torque as the magnetization direction is varied. A drastic difference in the behavior of the two types of torques results in a nontrivial evolution of switching properties with doping. Our findings promote the design of nonequilibrium orbital properties as the guiding mechanism for crafting the properties of spin-orbit torques in layered van der Waals materials.

DOI: [10.1103/PhysRevResearch.4.L042022](https://doi.org/10.1103/PhysRevResearch.4.L042022)

The discovery of two-dimensional (2D) van der Waals (vdW) ferromagnets Cr₂Ge₂Te₆ [1] and CrI₃ [2] has been long awaited since the works on how spatial dimensionality affects criticality [3,4]. Now, the potential applications of these discoveries seem vast within the field of spintronics [5]. A 2D layered material could enable the more efficient design of novel spintronic devices than their metallic bilayer counterparts with similar symmetries [6]. The recent discovery of Fe₃GeTe₂ (FGT) [7] stands as a significant milestone since its Curie temperature could be raised to room temperature with ionic liquid gating [8]. FGT has since been researched extensively, showing exciting characteristics such as nodal line semimetallicity [9], skyrmionic spin textures [10,11], and controllable spin currents [12]. In particular, experiments have demonstrated magnetization switching in Pt/FGT heterostructures via current-induced spin-orbit torque (SOT) [13,14].

We note that the magnetization switching demonstrated in Refs. [13,14] utilized the spin-Hall effect in Pt, where the physical principle is analogous to conventional SOT devices with transition-metal bilayers. A unique role played by the low crystal symmetry of FGT was pointed out by Johansen *et al.* [15], which allows for the generation of a current-induced torque without the need for a heavy metal interface. Experiments have now established the existence of such an unconventional torque [16,17]. However, these experiments were performed on bulklike thick samples $\gtrsim 20$ nm of FGT.

A key aspect of bulk FGT is the global inversion symmetry that prevents a net torque response. However, two vdW layers in the unit cell of bulk FGT, referred to as A and B layers, are inversion partners with respect to each other (see Fig. 1). Consequently, despite total torque vanishing, individual layers host local “staggered” torques. We note that a similar situation is encountered in other centrosymmetric systems, for which the concept of the “hidden” Rashba effect has been developed [18–20].

Although the symmetry dictates that current-induced torque in bulk FGT is similar to multiple copies of the result for monolayer FGT [16], the microscopic mechanism in bulk FGT is expected to be different from that of the monolayer. For instance, while current-induced torque in monolayer FGT will consist of both spin and orbital accumulations, in bulk FGT, spin and orbital currents exchanged between layers are also expected to contribute. In particular, recent theories predict that the orbital current can be generated much more efficiently than the spin current, e.g., via the orbital Hall effect, not only in transition metals [21–26] but also in 2D materials [27–29,29–31]. Moreover, the orbital current can exert torque on magnetic moments by transferring orbital angular momentum [32,33]. Known as the orbital torque, it provides a promising alternative route to control the magnetization through the orbital degree of freedom, and is considered a fresh perspective [34]. So far, the orbital torque has been experimentally observed mostly in transition-metal-based magnetic heterostructures [35–43]. However, owing to a highly anisotropic crystal field potential, strong spin-orbit coupling (SOC), and orbital complexity of the electronic structure, bulk FGT is expected to exhibit rich entangled dynamics between spin and orbital degrees of freedom. This motivates our search for the role of orbital excitations and its interaction with magnetic moments in bulk FGT, which will enhance the currently

*tsaunder@uni-mainz.de

Published by the American Physical Society under the terms of the [Creative Commons Attribution 4.0 International](https://creativecommons.org/licenses/by/4.0/) license. Further distribution of this work must maintain attribution to the author(s) and the published article's title, journal citation, and DOI.

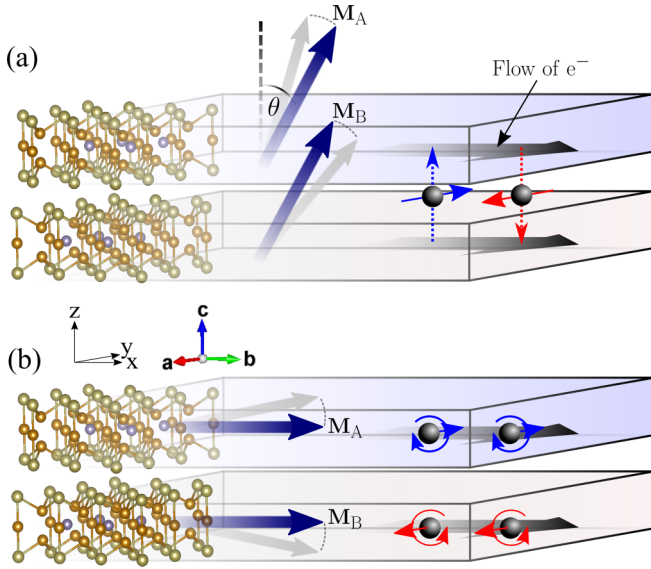


FIG. 1. A schematic illustration for current-induced torques in Fe_3GeTe_2 (FGT) with (a) an out-of-plane and (b) in-plane magnetization. In both instances the current direction is along the x axis. The crystal structure of Fe_3GeTe_2 , consisting of two individual layers, A and B, is displayed on the left. The direction of the magnetization at angle θ with the z axis is marked with \mathbf{M}_A and \mathbf{M}_B for each layer. The current-induced torques on each layer are opposite, so that the overall torque is vanishing. While for out-of-plane FGT, the magnetic torque is mainly driven by the flow of the spin angular momentum between layers [marked with arrows in (a)], the magnetic torque is dominated by prominent orbital accumulation for in-plane FGT [marked with arrows in (b)].

underdeveloped understanding of orbital physics in vdW materials.

In this Letter, by employing first-principles methods, we unveil the interplay of the spin and orbital angular momentum in bulk FGT, which is “hidden” by the global inversion symmetry. When the magnetization is pointing out of the vdW plane, we find spin flux exchanged between vdW layers is the major contribution to the torque on the magnetization [Fig. 1(a)]. In contrast, as the magnetization direction gets closer to the vdW plane, current-induced orbital accumulation becomes strongly pronounced, which leads to a large orbital torque response [Fig. 1(b)]. This is an example of an intrinsic crossover between spin and orbital torques, making bulk FGT an ideal candidate for studying nonequilibrium orbital excitations.

To describe the current-induced exchange of spin and orbital angular momentum between A and B layers, which results in torques on the magnetization, we adopt the spin continuity equation [33]

$$\frac{d\mathbf{S}_A}{dt} = \Phi_A + \mathcal{T}_{\text{SO},A} - \mathcal{T}_{\text{M},A}, \quad (1)$$

where the subscript stands for the vdW layer A. Here, Φ_A is the spin flux from layer B into layer A, $\mathcal{T}_{\text{SO},A} \sim \mathbf{L}_A \times \mathbf{S}_A$ describes mutual precession between the spin (\mathbf{S}_A) and orbital (\mathbf{L}_A) angular momenta at layer A via SOC, and $\mathcal{T}_{\text{M},A} \sim \hat{\mathbf{M}}_A \times \mathbf{S}_A$ is the torque that the spin \mathbf{S}_A exerts on A-layer magnetization \mathbf{M}_A through the exchange interaction. We re-

mark that the spin flux and local torques on layers A and B have the same magnitude but are opposite in sign by inversion symmetry. Thus, we analyze the dynamics of the A layer only and remove the subscript A in the following. In a steady state, when $d\mathbf{S}_A/dt = 0$, current-induced torque on the magnetization is given by two contributions: the spin flux Φ , and the angular momentum transfer from orbital to spin \mathcal{T}_{SO} . The latter originates from the orbital accumulation, hence we denote these as spin and orbital contributions to the magnetic torque, respectively. The magnetic torque in 2D systems is often described by nonequilibrium spin accumulation, but we emphasize that its origin is the nonequilibrium orbital angular momentum generation.

We assess the two contributions to the torque using a first-principles description of the system’s electronic structure, and Kubo formalism for electric field response \mathbf{E} , providing the details of our calculations in the Supplemental Material [44]. We use the code FLEUR [45], which implements the full-potential linearized augmented plane-wave method [46], in combination with Wannier interpolation [47,48] to efficiently compute the antidamping part of the torkance tensor \hat{T} defined as $\mathcal{T} = \hat{T} \mathbf{E}$. When represented in spherical coordinates we are interested only in the polar θ component of the torkance tensor, where θ is the angle that the magnetization makes with the z axis (see Fig. 1). Correspondingly, we assume simplified notations of T_M^θ , Φ^θ , and T_{SO}^θ for the θ component of the torkance tensor, and its spin flux and orbital parts. When studying the angular dependence of the torque, we consider only the case when the magnetization is tilted away from the z axis into the x axis while being kept in the xz plane. We apply the external electric field along x .

We first compute the magnitude of the total torkance and its decomposition in a single A layer of FGT as a function of angle θ , shown in Fig. 2(a). As predicted by symmetry [15], single-layer FGT hosts a nonvanishing SOT for $\theta \neq 0$. Interestingly, we find a sign change at $\theta \approx 60^\circ$ with the largest torkance when \mathbf{M} is in plane [Fig. 2(a)]. Markedly, the single-layer SOT is entirely orbital in origin as we find a complete lack of flux torkance for all magnetization angles. For the A layer in the bulk [Fig. 2(b)], the angular dependence has a similar functional form to single-layer FGT, with an overall suppression in magnitude. What stands in stark contrast to single-layer FGT is that the spin contribution Φ^θ constitutes a major component to the torque. This suggests that the bulk spin contribution may originate from the adjacent single-layer orbital contribution. However, as θ gets closer to 90° , the spin contribution Φ^θ is strongly suppressed and the orbital contribution T_{SO}^θ becomes dominant. This results in a peculiar angular dependence of the magnetic torque, which is significantly different from the prediction based on the leading-order symmetry expansion [15,49]. We also remark that bulk FGT is an example of a material exhibiting orbital-spin crossover of the magnetic torque as a function of magnetization angle. This can be attributed to the 2D nature of the crystal structure, which results in a highly anisotropic electronic structure.

In order to understand the origins of spin and orbital contributions to the magnetic torque, we calculate nonequilibrium spin and orbital accumulation induced by an external electric field, shown in Fig. 2(c) for the y component which is relevant for T_M^θ . For small values of θ , both S_y and L_y are proportional

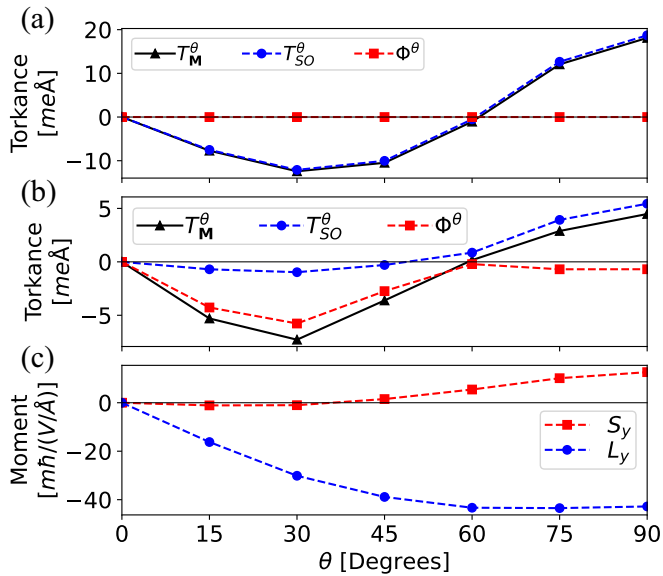


FIG. 2. Angular dependence of current-induced torque and the spin and orbital contributions in FGT. (a) The θ component of the antidamping current-induced torque on the magnetization (T_M^θ , black triangles), the spin contribution (Φ^θ , red dashed square), and the orbital contribution (T_{SO}^θ , blue dashed circle) for single-layer FGT as a function of θ . (b) Same as in (a) for the torqance projected onto the A layer in bulk FGT. (c) The y component of the current-induced orbital (L_y , blue dashed circle) and spin (S_y , red dashed square) moment summed over Fe atoms in the A layer of bulk FGT as a function of the angle θ .

to M_x , which is consistent with a symmetry analysis in the lowest order of \mathbf{M} [15]. However, as θ increases, higher-order contributions become more pronounced. Interestingly, S_y and L_y exhibit a qualitatively different angular dependence: S_y changes sign when θ is between 30° and 45° , while L_y monotonically increases as θ increases. Moreover, L_y is an

order of magnitude larger than S_y over a wide range of θ . This strongly supports the idea that orbital accumulation significantly contributes to the magnetic torque, especially for large values of θ . To understand why for smaller angles the orbital accumulation does not translate into a large orbital torque, we proceed to investigate the state-resolved properties to shed light on the microscopics of the crossover behavior.

We analyze band-resolved contributions to T_M^θ for $\theta = 30^\circ$ [Fig. 3(a)] and 90° [Fig. 3(b)]. These two angles are chosen such that they exhibit the strongest Φ^θ and T_{SO}^θ , respectively. As expected, the distributions of T_M^θ for $\theta = 30^\circ$ and $\theta = 90^\circ$ are qualitatively different. In particular, we find that the torque is spread over wider regions of phase space for $\theta = 30^\circ$, while for $\theta = 90^\circ$ the torque originates from isolated contributions, especially for energies above the Fermi level. To characterize the role of orbital accumulation we plot the state-resolved $L_{y,nk}$ at $\theta = 30^\circ$ [Fig. 3(c)] and $\theta = 90^\circ$ [Fig. 3(d)]. By comparing Figs. 3(a) and 3(c), we immediately notice that the isolated hotspotlike regions for T_M^θ and L_y at $\theta = 30^\circ$ are either not in the same position or have a different sign, which is especially visible around the Fermi energy. This is expected from Fig. 2(b) because the magnetic torque is dominated by the spin flux at $\theta = 30^\circ$. On the other hand, at $\theta = 90^\circ$ the correlation between T_M^θ and L_y is much more pronounced [compare Figs. 3(b) and 3(d)].

To understand the suppression of orbital torque despite the prominent current-induced orbital magnetization of states at small angles, we compare the \mathbf{k} -resolved contribution for L_y summed over all occupied states at $\theta = 30^\circ$ [Fig. 3(g)] and $\theta = 90^\circ$ [Fig. 3(h)]. While the summation over \mathbf{k} leads to an overall orbital moment at $\theta = 30^\circ$, the orbital moment at $\theta = 90^\circ$ is evidently greater, fitting with Fig. 2(c). Furthermore, there is asymmetry present at $\theta = 30^\circ$ that is not at $\theta = 90^\circ$, implying a crossover of orbital characters that could drive the orbital torque. The corresponding asymmetry of the orbital distribution for $\theta = 30^\circ$ can be also directly seen in the band structure plot for energies above the Fermi level

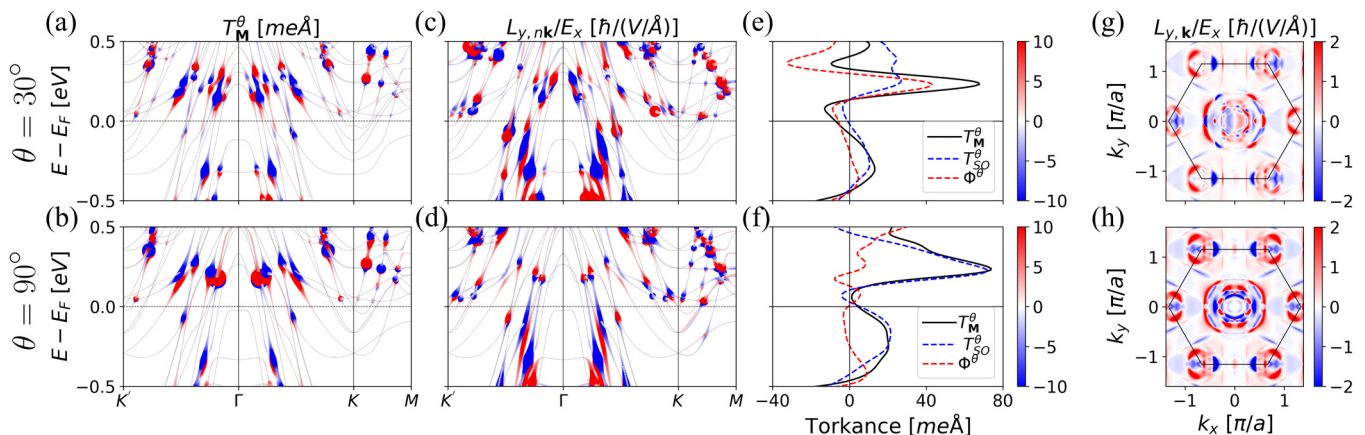


FIG. 3. Properties of the current-induced torque and orbital angular momentum of the A layer of Fe_3GeTe_2 for the magnetization angle of $\theta = 30^\circ$ [(a), (c), (e), (g)] and $\theta = 90^\circ$ [(b), (d), (f), (h)]. In (a) and (b) the plotted band structure is superimposed with the colored circles whose color and size represent the expectation value of the total torqance $T_{M,nk}^\theta$. Similarly, in (c) and (d) it is the y component of the current-induced orbital angular momentum $L_{y,nk}$ which is represented with the circles. Additionally, the \mathbf{k} -space distribution of $L_{y,k}$ for the two angles is shown in (g) and (h). (e) and (f) display the total integrated (T_M^θ , solid line), flux (Φ^θ , red dashed line), and orbital (T_{SO}^θ , blue dashed line) torqance as a function of band filling for (e) $\theta = 30^\circ$ and (f) $\theta = 90^\circ$, where $E = 0$ represents the true Fermi energy of FGT. The prominent current-induced orbital angular momentum and orbital torque for the in-plane magnetization is evident.

[Fig. 3(c)]. Conversely, the corresponding current induced spin distribution, presented in Supplemental Material [44], displays the opposite behavior. These findings help us understand the intricate energy-dependent interplay between the spin and orbital components to the magnetic torque as a function of the tilting angle.

In previous works, the effect of strong correlations using dynamical mean-field theory have been investigated [9]. Within the energy range chosen in our investigation, the only key difference between both methods is the position of the Fermi level. Hence, we show the Fermi energy dependence of T_M^θ , Φ^θ , and T_{SO}^θ at $\theta = 30^\circ$ and 90° in Figs. 3(e) and 3(f), respectively. At $\theta = 30^\circ$, Φ^θ is the main contribution to T_M^θ although T_{SO}^θ is also nonvanishing [Fig. 3(e)]. On the other hand, at $\theta = 90^\circ$, T_M^θ is mainly governed by T_{SO}^θ and Φ^θ is suppressed over a wide energy range [Fig. 3(f)]. In Figs. 3(a)–3(d), we notice that the hotspots are mainly concentrated around the nodal lines near Γ at +0.2 eV [9]. This implies that the torkance can be efficiently tuned with band filling. Indeed, we find a substantial increase of T_M^θ as the Fermi energy is raised by ~ 0.2 eV at both $\theta = 30^\circ$ and 90° . Interestingly, at $\theta = 30^\circ$, T_M^θ changes sign from negative to positive as the Fermi energy is increased by ≈ 0.2 eV. On the other hand, at $\theta = 90^\circ$, the sign of T_M^θ remains positive. This suggests a possibility of tuning the sign and magnitude of the torkance by doping. Such complex anisotropic torkances can be harnessed to drive the nontrivial excitations of spin textures that FGT hosts [50]. According to our estimate, raising the energy by 0.2 eV requires ≈ 1.5 additional electrons per layer. This may be achieved, e.g., by substitutional doping of Fe by Co.

Let us comment lastly on the relevance of our predictions for the spin-orbit torque measurements on realistic FGT samples. While the single-layer SOT in bulk samples can be promoted if global symmetry is broken, e.g., by surfaces and interfaces [16,17], inversion symmetry present in ideal bulk FGT ultimately suppresses the overall torque on the magnetization. However, the reality is that there are a variety of “intrinsic” mechanisms which can drive the inversion symmetry breaking in this bulk system [17,51,52]. One of these effects is that of magnetostriction [51]. Here, due to the coupling of the lattice to the magnetic moment, the rotation of the moment can initiate a crystal structure change, breaking the inversion symmetry of the perfect crystal. Similarly, the effects of the electric field on the system could give rise to high-frequency magnon modes capable of canting the spins and driving a torque even in the pristine limit. It is also plausible to assume that due to the 2D vdW nature of the material it is possible for the layers to slip over one another. In some instances, if multiple pairs of layers have displaced in different

ways, the inversion symmetry could be broken in this fashion. Moreover, recent experimental work reports a discrepancy in the occupancy of the central Fe atom in the A layer versus the B layer [52]. This implies that the unit cell is no longer inversion symmetric providing an avenue for bulk torque generation. Our results can be in principle readily applied to this situation: Due to the interlayer occupancy difference being small, from the theoretical perspective the corresponding torque should be simply given by the difference in the torques of layers A and B from Figs. 3(e) and 3(f) for corresponding occupancies, and the corresponding effective spin-orbit field can be found in a similar fashion [15].

Finally, the determination of the components of the spin and orbital torque remains a significant challenge. For example, standard techniques for measuring the current-induced torques only measure the total torkance, but this can be overcome by attempting to find an “even”-“odd” effect such as in MoS₂ [30] by consecutively removing vdW layers. To probe the orbital accumulation, a key signature of orbital-driven torkances, one can use optical probes such as magneto-optical Kerr effect [53] or x-ray magnetic circular dichroism [54].

To summarize, in our Letter, we uncovered that in magnetic vdW materials the microscopics of spin-orbit torques can be extremely rich owing to the pronounced 2D nature of constituting layers and their orbital complexity. As we show for FGT, this ultimately results in profoundly anisotropic torque properties, which may be mediated by an exotic orbital-spin crossover. Given the fundamentally different properties of spin and orbital angular momentum out of equilibrium, this suggests exciting possibilities in exploring spin-orbital dynamics of 2D magnets and corresponding transport manifestations. We further argue that the detailed knowledge of “hidden” spin-orbit torques in bulk vdW materials can provide a key to designing their current response via educated symmetry breaking, which may prove pivotal for the integration of 2D magnets into the spintronic device setting.

The authors appreciate fruitful discussions with Professor Arne Brataas, Dr. Martin Gradhand, Maximilian Merte, Fabian Lux, and Dr. Sumit Ghosh. We gratefully acknowledge the Jülich Supercomputing Centre for providing computational resources under Project No. jiff40. This work was funded by the Deutsche Forschungsgemeinschaft (DFG, German Research Foundation) Grants No. TRR 173/2-268565370 Spin+X (Projects No. A01, No. B02, and No. A11), No. TRR 288-422213477 (Project No. B06), and CRC 1238-277146847 (Project No. C01). M.K. acknowledges support by the research Council of Norway through its Centers of Excellence funding scheme, project number 202633 “QuSpin”.

- [1] C. Gong, L. Li, Z. Li, H. Ji, A. Stern, Y. Xia, T. Cao, W. Bao, C. Wang, Y. Wang, Z. Q. Qiu, R. J. Cava, S. G. Louie, J. Xia, and X. Zhang, Discovery of intrinsic ferromagnetism in two-dimensional van der Waals crystals, *Nature (London)* **546**, 265 (2017).
- [2] B. Huang, G. Clark, E. Navarro-Moratalla, D. R. Klein, R. Cheng, K. L. Seyler, D. Zhong, E. Schmidgall, M. A. McGuire,

D. H. Cobden, W. Yao, D. Xiao, P. Jarillo-Herrero, and X. Xu, Layer-dependent ferromagnetism in a van der Waals crystal down to the monolayer limit, *Nature (London)* **546**, 270 (2017).

- [3] R. B. Griffiths, Peierls proof of spontaneous magnetization in a two-dimensional Ising ferromagnet, *Phys. Rev.* **136**, A437 (1964).

- [4] N. D. Mermin and H. Wagner, Absence of Ferromagnetism or Antiferromagnetism in One- or Two-Dimensional Isotropic Heisenberg Models, *Phys. Rev. Lett.* **17**, 1133 (1966).
- [5] G. Hu and B. Xiang, Recent advances in two-dimensional spintronics, *Nanoscale Res. Lett.* **15**, 226 (2020).
- [6] L. Liu, C. Zhou, X. Shu, C. Li, T. Zhao, W. Lin, J. Deng, Q. Xie, S. Chen, J. Zhou, R. Guo, H. Wang, J. Yu, S. Shi, P. Yang, S. Pennycook, A. Manchon, and J. Chen, Symmetry-dependent field-free switching of perpendicular magnetization, *Nat. Nanotechnol.* **16**, 277 (2021).
- [7] H. J. Deiseroth, K. Aleksandrov, C. Reiner, L. Kienle, and R. K. Kremer, Fe_3GeTe_2 and Ni_3GeTe_2 —two new layered transition-metal compounds: Crystal structures, HRTEM investigations, and magnetic and electrical properties, *Eur. J. Inorg. Chem.* **2006**, 1561 (2006).
- [8] Y. Deng, Y. Yu, Y. Song, J. Zhang, N. Z. Wang, Z. Sun, Y. Yi, Y. Z. Wu, S. Wu, J. Zhu, J. Wang, X. H. Chen, and Y. Zhang, Gate-tunable room-temperature ferromagnetism in two-dimensional Fe_3GeTe_2 , *Nature (London)* **563**, 94 (2018).
- [9] K. Kim, J. Seo, E. Lee, K. T. Ko, B. S. Kim, B. G. Jang, J. M. Ok, J. Lee, Y. J. Jo, W. Kang, J. H. Shim, C. Kim, H. W. Yeom, B. Il Min, B. J. Yang, and J. S. Kim, Large anomalous Hall current induced by topological nodal lines in a ferromagnetic van der Waals semimetal, *Nat. Mater.* **17**, 794 (2018).
- [10] B. Ding, Z. Li, G. Xu, H. Li, Z. Hou, E. Liu, X. Xi, F. Xu, Y. Yao, and W. Wang, Observation of magnetic skyrmion bubbles in a van der Waals ferromagnet Fe_3GeTe_2 , *Nano Lett.* **20**, 868 (2020).
- [11] T. E. Park, L. Peng, J. Liang, A. Hallal, F. S. Yasin, X. Zhang, K. M. Song, S. J. Kim, K. Kim, M. Weigand, G. Schütz, S. Finizio, J. Raabe, K. Garcia, J. Xia, Y. Zhou, M. Ezawa, X. Liu, J. Chang, H. C. Koo *et al.*, Néel-type skyrmions and their current-induced motion in van der Waals ferromagnet-based heterostructures, *Phys. Rev. B* **103**, 104410 (2021).
- [12] J. Zhou and J. C. Charlier, Controllable spin current in van der Waals ferromagnet Fe_3GeTe_2 , *Phys. Rev. Res.* **3**, L042033 (2021).
- [13] M. Alghamdi, M. Lohmann, J. Li, P. R. Jothi, Q. Shao, M. Aldosary, T. Su, B. P. T. Fokwa, and J. Shi, Highly efficient spin-orbit torque and switching of layered ferromagnet Fe_3GeTe_2 , *Nano Lett.* **19**, 4400 (2019).
- [14] Y. Zhang, H. Xu, C. Yi, X. Wang, Y. Huang, J. Tang, J. Jiang, C. He, M. Zhao, T. Ma, J. Dong, C. Guo, J. Feng, C. Wan, H. Wei, H. Du, Y. Shi, G. Yu, G. Zhang, and X. Han, Exchange bias and spin-orbit torque in the Fe_3GeTe_2 -based heterostructures prepared by vacuum exfoliation approach, *Appl. Phys. Lett.* **118**, 262406 (2021).
- [15] Ø. Johansen, V. Risinggård, A. Sudbø, J. Linder, and A. Brataas, Current Control of Magnetism in Two-Dimensional Fe_3GeTe_2 , *Phys. Rev. Lett.* **122**, 217203 (2019).
- [16] K. Zhang, S. Han, Y. Lee, M. J. Coak, J. Kim, I. Hwang, S. Son, J. Shin, M. Lim, D. Jo, K. Kim, D. Kim, H. W. Lee, and J. G. Park, Gigantic current control of coercive field and magnetic memory based on nanometer-thin ferromagnetic van der Waals Fe_3GeTe_2 , *Adv. Mater.* **33**, 2004110 (2021).
- [17] F. Martin, K. Lee, M. Schmitt, A. Liedtke, A. Shahee, H. T. Simensen, T. Scholz, T. G. Saunderson, D. Go, M. Gradhand, Y. Mokrousov, T. Denneulin, A. Kovács, B. Lotsch, A. Brataas, and M. Kläui, Strong bulk spin-orbit torques quantified in the van der Waals ferromagnet Fe_3GeTe_2 , *Mater. Res. Lett.* **11**, 84 (2022).
- [18] L. Yuan, Q. Liu, X. Zhang, J. W. Luo, S. S. Li, and A. Zunger, Uncovering and tailoring hidden Rashba spin-orbit splitting in centrosymmetric crystals, *Nat. Commun.* **10**, 906 (2019).
- [19] W. A. Atkinson, Microscopic model for the hidden Rashba effect in $\text{YBa}_2\text{Cu}_3\text{O}_{6+x}$, *Phys. Rev. B* **101**, 024513 (2020).
- [20] S. Lee and Y. K. Kwon, Unveiling giant hidden Rashba effects in two-dimensional Si_2Bi_2 , *npj 2D Mater. Appl.* **4**, 45 (2020).
- [21] H. Kontani, T. Tanaka, D. S. Hirashima, K. Yamada, and J. Inoue, Giant Intrinsic Spin and Orbital Hall Effects in Sr_2MO_4 ($M = \text{Ru, Rh, Mo}$), *Phys. Rev. Lett.* **100**, 096601 (2008).
- [22] H. Kontani, T. Tanaka, D. S. Hirashima, K. Yamada, and J. Inoue, Giant Orbital Hall Effect in Transition Metals: Origin of Large Spin and Anomalous Hall Effects, *Phys. Rev. Lett.* **102**, 016601 (2009).
- [23] D. Go, D. Jo, C. Kim, and H. W. Lee, Intrinsic Spin and Orbital Hall Effects from Orbital Texture, *Phys. Rev. Lett.* **121**, 086602 (2018).
- [24] D. Jo, D. Go, and H. W. Lee, Gigantic intrinsic orbital Hall effects in weakly spin-orbit coupled metals, *Phys. Rev. B* **98**, 214405 (2018).
- [25] L. Salemi and P. M. Oppeneer, First-principles theory of intrinsic spin and orbital Hall and Nernst effects in metallic monoatomic crystals, *Phys. Rev. Mater.* **6**, 095001 (2022).
- [26] L. Salemi and P. M. Oppeneer, Theory of magnetic spin and orbital Hall and Nernst effects in bulk ferromagnets, *Phys. Rev. B* **106**, 024410 (2022).
- [27] L. M. Canonico, T. P. Cysne, A. Molina-Sanchez, R. B. Muniz, and T. G. Rappoport, Orbital Hall insulating phase in transition metal dichalcogenide monolayers, *Phys. Rev. B* **101**, 161409(R) (2020).
- [28] L. M. Canonico, T. P. Cysne, T. G. Rappoport, and R. B. Muniz, Two-dimensional orbital Hall insulators, *Phys. Rev. B* **101**, 075429 (2020).
- [29] S. Bhowal and S. Satpathy, Intrinsic orbital and spin Hall effects in monolayer transition metal dichalcogenides, *Phys. Rev. B* **102**, 035409 (2020).
- [30] T. P. Cysne, M. Costa, L. M. Canonico, M. B. Nardelli, R. B. Muniz, and T. G. Rappoport, Disentangling Orbital and Valley Hall Effects in Bilayers of Transition Metal Dichalcogenides, *Phys. Rev. Lett.* **126**, 056601 (2021).
- [31] S. Bhowal and G. Vignale, Orbital Hall effect as an alternative to valley Hall effect in gapped graphene, *Phys. Rev. B* **103**, 195309 (2021).
- [32] D. Go and H.-W. Lee, Orbital torque: Torque generation by orbital current injection, *Phys. Rev. Res.* **2**, 013177 (2020).
- [33] D. Go, F. Freimuth, J. P. Hanke, F. Xue, O. Gomonay, K. J. Lee, S. Blügel, P. M. Haney, H. W. Lee, and Y. Mokrousov, Theory of current-induced angular momentum transfer dynamics in spin-orbit coupled systems, *Phys. Rev. Res.* **2**, 033401 (2020).
- [34] D. Go, D. Jo, H.-W. Lee, M. Kläui, and Y. Mokrousov, Orbital currents in solids, *Europhys. Lett.* **135**, 37001 (2021).
- [35] S. Ding, A. Ross, D. Go, L. Baldrati, Z. Ren, F. Freimuth, S. Becker, F. Kammerbauer, J. Yang, G. Jakob, Y. Mokrousov, and M. Kläui, Harnessing Orbital-to-Spin Conversion of Interfacial

- Orbital Currents for Efficient Spin-Orbit Torques, *Phys. Rev. Lett.* **125**, 177201 (2020).
- [36] J. Kim, D. Go, H. Tsai, D. Jo, K. Kondou, H.-W. Lee, and Y. Otani, Nontrivial torque generation by orbital angular momentum injection in ferromagnetic-metal/Cu/Al₂O₃ trilayers, *Phys. Rev. B* **103**, L020407 (2021).
- [37] D. Lee, D. Go, H.-J. Park, W. Jeong, H.-W. Ko, D. Yun, D. Jo, S. Lee, G. Go, J. H. Oh, K.-J. Kim, B.-G. Park, B.-C. Min, H. C. Koo, H.-W. Lee, O. Lee, and K.-J. Lee, Orbital torque in magnetic bilayers, *Nat. Commun.* **12**, 6710 (2021).
- [38] S. Lee, M.-G. Kang, D. Go, D. Kim, J.-H. Kang, T. Lee, G.-H. Lee, J. Kang, N. J. Lee, Y. Mokrousov, S. Kim, K.-J. Kim, K.-J. Lee, and B.-G. Park, Efficient conversion of orbital hall current to spin current for spin-orbit torque switching, *Commun. Phys.* **4**, 234 (2021).
- [39] S. Ding, Z. Liang, D. Go, C. Yun, M. Xue, Z. Liu, S. Becker, W. Yang, H. Du, C. Wang, Y. Yang, G. Jakob, M. Kläui, Y. Mokrousov, and J. Yang, Observation of the Orbital Rashba-Edelstein Magnetoresistance, *Phys. Rev. Lett.* **128**, 067201 (2022).
- [40] L. Liao, F. Xue, L. Han, J. Kim, R. Zhang, L. Li, J. Liu, X. Kou, C. Song, F. Pan, and Y. Otani, Efficient orbital torque in polycrystalline ferromagnetic-metal/Ru/Al₂O₃ stacks: Theory and experiment, *Phys. Rev. B* **105**, 104434 (2022).
- [41] C.-Y. Hu, Y.-F. Chiu, C.-C. Tsai, C.-C. Huang, K.-H. Chen, C.-W. Peng, C.-M. Lee, M.-Y. Song, Y.-L. Huang, S.-J. Lin, and C.-F. Pai, Toward 100% spin-orbit torque efficiency with high spin-orbital Hall conductivity Pt-Cr alloys, *ACS Appl. Electron. Mater.* **4**, 1099 (2022).
- [42] H. Hayashi, D. Jo, D. Go, Y. Mokrousov, H.-W. Lee, and K. Ando, Observation of long-range orbital transport and giant orbital torque, [arXiv:2202.13896](https://arxiv.org/abs/2202.13896).
- [43] E. Santos, J. E. Abrão, D. Go, L. K. de Assis, J. B. S. Mendes, and A. Azevedo, Inverse orbital torque via spin-orbital entangled states, [arXiv:2204.01825](https://arxiv.org/abs/2204.01825).
- [44] See Supplemental Material at <http://link.aps.org/supplemental/10.1103/PhysRevResearch.4.L042022> for the full theoretical method, computational details and numerical parameters for each stage of the calculation. In addition, some further figures including crystal structure, additional Fermi surface textures and comparisons to other methods, which includes Refs. [9,14,15,17,33,45–48,55–57].
- [45] For the program description, see <https://www.flapw.de>.
- [46] E. Wimmer, H. Krakauer, M. Weinert, and A. J. Freeman, Full-potential self-consistent linearized-augmented-plane-wave method for calculating the electronic structure of molecules and surfaces: O₂ molecule, *Phys. Rev. B* **24**, 864 (1981).
- [47] F. Freimuth, Y. Mokrousov, D. Wortmann, S. Heinze, and S. Blügel, Maximally localized Wannier functions within the FLAPW formalism, *Phys. Rev. B* **78**, 035120 (2008).
- [48] G. Pizzi, V. Vitale, R. Arita, S. Blügel, F. Freimuth, G. Géranton, M. Gibertini, D. Gresch, C. Johnson, T. Koretsune, J. Ibañez-Azpiroz, H. Lee, J. M. Lihm, D. Marchand, A. Marrazzo, Y. Mokrousov, J. I. Mustafa, Y. Nohara, Y. Nomura, L. Paulatto *et al.*, Wannier90 as a community code: New features and applications, *J. Phys.: Condens. Matter* **32**, 165902 (2020).
- [49] H. Kurebayashi, J. H. Garcia, S. Khan, J. Sinova, and S. Roche, Magnetism, symmetry and spin transport in van der Waals layered systems, *Nat. Rev. Phys.* **4**, 150 (2022).
- [50] J. P. Hanke, F. Freimuth, B. Dupé, J. Sinova, M. Kläui, and Y. Mokrousov, Engineering the dynamics of topological spin textures by anisotropic spin-orbit torques, *Phys. Rev. B* **101**, 014428 (2020).
- [51] F. Narita and M. Fox, A review on piezoelectric, magnetostrictive, and magnetoelectric materials and device technologies for energy harvesting applications, *Adv. Eng. Mater.* **20**, 1700743 (2018).
- [52] A. Chakraborty, A. K. Srivastava, A. K. Sharma, A. K. Gopi, K. Mohseni, A. Ernst, H. Deniz, B. K. Hazra, S. Das, P. Sessi, I. Kostanovskiy, T. Ma, H. L. Meyerheim, and S. S. P. Parkin, Magnetic skyrmions in a thickness tunable 2D ferromagnet from a defect driven Dzyaloshinskii-Moriya interaction, *Adv. Mater.* **34**, 2108637 (2022).
- [53] Y.-G. Choi, D. Jo, K.-H. Ko, D. Go, K.-H. Kim, H. G. Park, C. Kim, B.-C. Min, G.-M. Choi, and H.-W. Lee, Observation of the orbital Hall effect in a light metal Ti, [arXiv:2109.14847](https://arxiv.org/abs/2109.14847).
- [54] C. Stamm, C. Murer, Y. Acremann, M. Baumgartner, R. Gort, S. Däster, A. Kleibert, K. Gareilo, J. Feng, M. Gabureac, Z. Chen, J. Stöhr, and P. Gambardella, X-ray spectroscopy of current-induced spin-orbit torques and spin accumulation in Pt/3d-transition-metal bilayers, *Phys. Rev. B* **100**, 024426 (2019).
- [55] J. P. Perdew, K. Burke, and M. Ernzerhof, Generalized Gradient Approximation Made Simple, *Phys. Rev. Lett.* **77**, 3865 (1996).
- [56] Fe₃GeTe₂ Crystal Structure: Datasheet from PAULING FILE Multinaries Edition - 2012 in SpringerMaterials, edited by P. Villars and K. Cenzual, Springer, Berlin/Material Phases Data System (MPDS), Switzerland/National Institute for Materials Science (NIMS), Japan, 2016, https://materials.springer.com/isp/crystallographic/docs/sd_1420956.
- [57] X. Wang, J. R. Yates, I. Souza, and D. Vanderbilt, *Ab initio* calculation of the anomalous Hall conductivity by Wannier interpolation, *Phys. Rev. B* **74**, 195118 (2006).